electronic materials

Article

Structural Changes Induced by Heating in Sputtered NiO and Cr_2O_3 Thin Films as p-Type Transparent Conductive Electrodes

Cecilia Guillén and José Herrero

Special Issue
Feature Papers of Electronic Materials

Edited by
Prof. Dr. Wojciech Pisula

MDPI

https://doi.org/10.3390/electronicmat2020005

electronic materials

MDPI

Article

Structural Changes Induced by Heating in Sputtered NiO and Cr_2O_3 Thin Films as p-Type Transparent Conductive Electrodes

Cecilia Guillén * and José Herrero

Department of Energy, Centro de Investigaciones Energéticas Medioambientales y Tecnológicas (CIEMAT), Avda. Complutense 40, 28040 Madrid, Spain; jose.herrero@ciemat.es
* Correspondence: c.guillen@ciemat.es

Abstract: NiO and Cr_2O_3 are transition metal oxides with a partially filled d electron band that supports p-type conduction. Both are transparent to the visible light due to optical absorption beginning at wavelengths below 0.4 μm and the creation of holes by metal vacancy defects. The defect and strain effects on the electronic characteristics of these materials need to be established. For this purpose, NiO and Cr_2O_3 thin films were deposited on unheated glass substrates by reactive DC sputtering from metallic targets. Their structural, morphological, optical and electrical properties were analyzed comparatively in the as-grown conditions (25 °C) and after heating in air at 300 °C or 500 °C. The cubic NiO structure was identified with some tensile strain in the as-grown conditions and compressive strain after heating. Otherwise, the chromium oxide layers were amorphous as grown at 25 °C and crystallized into hexagonal Cr_2O_3 at 300 °C or above also with compressive strain after heating. Both materials achieved the highest visible transmittance (72%) and analogous electrical conductivity (~10^{-4} S/cm) by annealing at 500 °C. The as-grown NiO films showed a higher conductivity (2.5 × 10^{-2} S/cm) but lower transmittance (34%), which were related to more defects causing tensile strain in these samples.

Keywords: sputtering; thin films; optical transmittance; electrical conductivity

Citation: Guillén, C.; Herrero, J. Structural Changes Induced by Heating in Sputtered NiO and Cr_2O_3 Thin Films as p-Type Transparent Conductive Electrodes. *Electron. Mater.* **2021**, *2*, 49–59. https://doi.org/10.3390/electronicmat2020005

Academic Editor: Alicia de Andrés

Received: 6 February 2021
Accepted: 24 March 2021
Published: 29 March 2021

1. Introduction

Transparent conducting oxides (TCOs) are critical to numerous technological applications, ranging from flat panel displays or light emitting diodes to smart windows and photovoltaic cells [1,2]. The performances of p-type TCOs are behind the n-type counterparts, which limit potential applications in the field of transparent electronics [3]. This discrepancy stems from the localized nature of the O 2p-derived valence band (VB) in contrast with a spatially spread conduction band (CB) composed of metal s orbitals, which results in a much higher effective mass for holes than electrons [4] in addition to easy n-type dopability by oxygen vacancy defects [5]. A design strategy for p-type TCOs is based on the concept of chemical modulation of the VB through the hybridization of O 2p orbitals with metal d or s orbitals, which is advantageous for the mobility of holes [6]. Another approximation is to utilize the electron correlation to promote VB modifications that favor p-type conduction [7]. In this sense, many transition metal oxides with a partially filled d electron band are described by extended Hubbard models [8,9] where the Coulomb interaction between the electrons (U) splits the d band into an upper Hubbard band (UHB) and a lower Hubbard band (LHB) with a separation of U [10]. Consequently, these compounds can support p-type conduction when the VB is composed of O 2p orbitals and metal d orbitals (LHB) driven by the electron correlation.

Transition metal monoxides crystallize in the rock-salt structure and sesquioxides in the corundum structure, showing a similar trend of electronic properties: the values of U gradually decrease with the decrease of the 3d occupation number of the transition metal ion [11]. The electrical conductivity can be improved by decreasing U while maintaining the

consequence of the VB modification due to the electron correlation for p-type conduction. Although with differences in their electronic structure, NiO (Ni^{2+} $3d^8$) and Cr_2O_3 (Cr^{3+} $3d^3$) are equally suitable for acting as p-TCOs [6]. Both are transparent to the visible light due to optical absorption beginning at wavelengths below 0.4 μm and they allow the creation of holes by metal vacancy defects (V_{Ni} or V_{Cr}) [12,13].

Due to its lower 3d occupation number, a lower *U* and higher electrical conductivity are expected for Cr_2O_3 than NiO. Nevertheless, the respective electronic characteristics can be altered as previous studies have revealed that compressive strain can increase the band gap energy and *U* values in both Cr_2O_3 [13] and NiO [14]. In addition, the metal vacancy defects play an important role in changing the lattice arrangement and introducing charge transition levels that modify the electronic bands [15,16]. The defect and strain effects on the electronic characteristics of these p-type TCOs need to be established in relation to the specific preparation procedure. For this purpose, NiO and Cr_2O_3 thin films were deposited on unheated glass substrates by reactive DC sputtering from metallic targets. This is a good technique for the preparation of metal oxide layers with a low cost due to simple equipment and easy extrapolation to large areas [17] and it is used here for the synthesis of compounds that are practically nontoxic [18] although source metals and potential by-products (such as Cr^{6+} species) are problematic. The structural, morphological, optical and electrical properties of the sputtered films were comparatively analyzed in the as-grown conditions (25 °C) and after heating in air at 300 °C or 500 °C, thus studying the evolution of their characteristics with temperature. The main objective was to elucidate the structural effects on the transparency and conductivity of NiO and Cr_2O_3 thin films prepared under analogous conditions by a low cost and easily scalable deposition technique.

2. Materials and Methods

Nickel oxide and chromium oxide thin films were prepared on unheated soda-lime glass substrates (2 mm thick) by reactive DC magnetron sputtering from Ni and Cr targets, respectively. After the evacuation of the chamber to a base pressure of 4×10^{-4} Pa, the reactive and working gases (O_2 and Ar) were introduced by independent mass flow controllers. The O_2 to Ar partial pressure ratio was selected to obtain near stoichiometric NiO and Cr_2O_3 layers according to previous studies [12,19,20] while the power density was adjusted to get a deposition rate of 20 nm/min for the various films, as detailed in Table 1. For the analogous nickel oxide layers, a previous work showed the evolution of the cation coordination number (N_c) with the oxygen partial pressure being the stoichiometric value ($N_c = 6$) achieved at $P(O_2)/P(O_2 + Ar) = 0.2$ [12]. For the chromium oxide samples, several oxygen pressures were also tested and the set value corresponded with the intermediate range between the metallic mode (opaque films) at $P(O_2)/P(O_2 + Ar) \leq 0.3$ and the oxidative mode (with the poisoning of the target [19]) at $P(O_2)/P(O_2 + Ar) \geq 0.5$.

Table 1. Experimental conditions of sputtering deposition.

Target (Ø 15 cm)	P_{base} (Pa)	$P(O_2)$ (Pa)	$P(O_2 + Ar)$ (Pa)	Power (W/cm^2)
Ni disk	4×10^{-4}	0.10	0.50	2
Cr disk	4×10^{-4}	0.20	0.50	12

The thickness of each layer was measured after deposition with a Dektak 3030 profilometer (Veeco Instruments GmbH, Mannheim, Germany). This value and the corresponding deposition time were used to calculate the growth rate and adjust the power density accordingly. Once the rate of 20 nm/min was reached, the deposition time was set at 5 min to obtain layers with a same thickness of 100 nm. In order to improve the crystallinity of the sputtered samples, post-deposition heat treatments were performed in air at temperatures ranging from 300 °C to 500 °C for 30 min.

The crystallographic properties were examined by X-ray diffraction (XRD) with radiation Cu $K_{\alpha 1}$ ($\lambda = 1.54056$ Å) in an X'Pert instrument (PANalytical, Malvern, UK) with

a Bragg–Brentano θ–2θ configuration. The crystalline phases were identified by the files given by the Joint Committee of Powder Diffraction Standards (JCPDS) and the mean crystallite size was calculated from the full width at half the maximum of the main diffraction peak according to the Scherrer formula. The microstructure of the films was also analyzed with a system composed of a BAC151B microscope and an i-Raman spectrometer (B&W Tek, Newark, NJ, USA) using a green laser of 532 nm as the excitation source. The topography was examined by atomic force microscopy (AFM) with a Park XE-100 (Park Systems, Suwon, Korea) in contact mode, acquiring digital images to quantify the surface roughness. For the optical characterization, transmittance (T) and reflectance (R) measurements were done with a double beam spectrophotometer Lambda 9 (PerkinElmer Inc., Waltham, MA, USA) in the wavelength range λ = 0.3–1.9 μm taking the air as the reference. The transmittance was then corrected for reflection losses as $T_c(\%) = 100\ T(\%)/(100 - R(\%))$. This was directly related to the optical absorption coefficient $\alpha = -(1/t)\ \ln(T_c/100)$ [21] being $T_c \approx 100\%$ below the band gap energy E_g where $\alpha \approx 0$. Thus, the E_g value could be determined as the maximum of the differential $d\alpha/dE$ or dT_c/dE versus the light energy E [22]. The electrical conductivity together with carrier concentration and mobility were determined with an HMS3000 Hall Measurement System (ECOPIA, Gyeonggi-do, Korea) using the Van der Pauw configuration and a magnetic field of 0.5 T. Silver paste contacts with a 1 mm diameter size were placed at the four corners of the sample (1 cm × 1 cm) and four measurements (with the bias applied in different diagonal directions and reversing the field) were taken of each layer. The sheet resistance (R_s) was also obtained with a four-point probe VEECO FPP5000 (Veeco Instruments Inc., Plainview, NY, USA) showing a complete agreement with the equation $R_s = (\sigma \cdot t)^{-1}$ where σ was the Hall conductivity and t was the film thickness.

3. Results and Discussion

An XRD analysis conducted on the various samples is illustrated in Figure 1. All of the nickel oxide layers showed diffraction peaks corresponding with the cubic rock-salt structure of NiO (JCPDS No. 4-835). A mean crystallite size of 40 nm was obtained for the as-grown films with a lattice constant a = 0.420 nm that was higher than expected from the standard powder file (0.418 nm) [12]. Such enlargement in the lattice was related to the presence of nickel vacancies $(V_{Ni})^{2-}$ and the concurrent formation of some Ni^{3+} to preserve electrical neutrality. The coexistence of Ni^{2+} and Ni^{3+} produced a local spinel arrangement (as in a mixed valence Ni_3O_4 [23]) dispersed in the NiO matrix, which altered the cubic rock-salt structure and increased the lattice parameter [24]. During heating in air at 300 °C or 500 °C, NiO crystallites enlarged slightly to 45 nm while the lattice constant decreased to a = 0.416 nm. Otherwise, no diffraction peaks were observed for the as-grown chromium oxide samples, indicating that they were amorphous as reported for analogous layers prepared at room temperature [25,26]. After heating at 300 °C or above, diffraction peaks evidenced hexagonal Cr_2O_3 (JCPDS 72-3533) with a mean crystallite size of 55 nm and lattice parameters a = 0.492 nm and c = 1.359 nm. These gave a unit cell volume lower than expected from the standard powder file (0.495 nm and 1.358 nm cell parameters) [27] without significant changes with the annealing temperature. At 300 °C, some Cr_2O_5 (JCPDS 28-0370) also appeared that was related to the coexistence of Cr^{3+} and Cr^{6+} by the combination of CrO_8 octahedra and CrO_4 tetrahedra [28]. This is a metastable compound favored by the presence of chromium (III) vacancies $(V_{Cr})^{3-}$ together with Cr^{6+} species but Cr_2O_5 decomposes into Cr_2O_3 around 400 °C [29,30]. In fact, pure Cr_2O_3 is typically synthetized at temperatures above 450 °C [19,29]. The presence of Cr_2O_5 in the 300 °C heated sample produced some screening of the (012) Cr_2O_3 diffraction, which was located between two peaks corresponding with Cr_2O_5. It should be noted that a similar evolution has been observed by increasing the heating temperature during sputter deposition [31,32]. However, the film growth rate tends to decrease as the substrate temperature increases [31]. Sputtering on unheated substrates allows the minimisation of

the power required for the stated deposition rate and the film thickness remains unchanged after post-deposition heating.

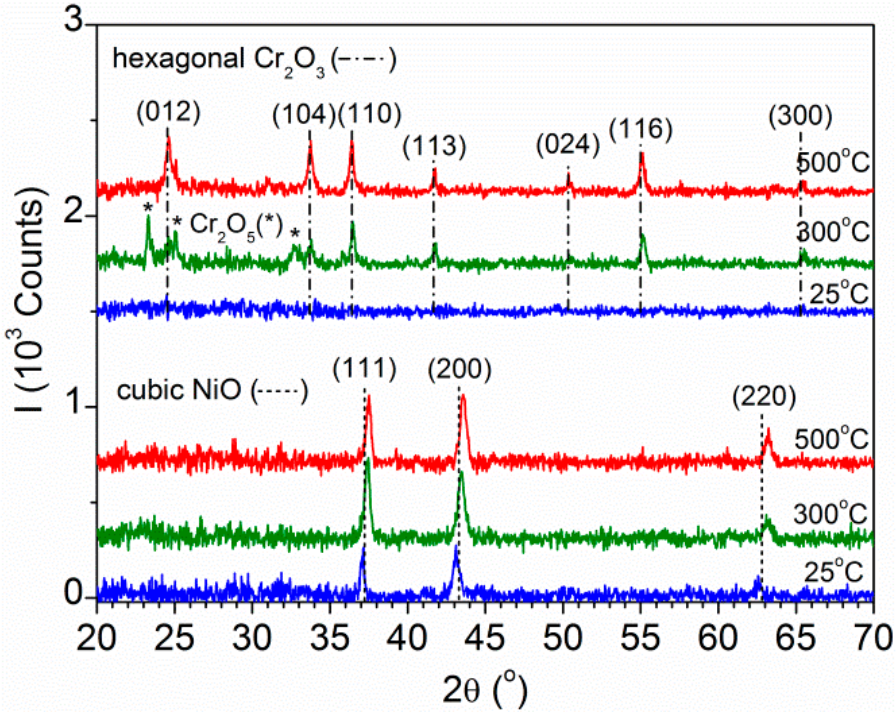

Figure 1. XRD patterns corresponding with the nickel oxide and chromium oxide samples as grown at room temperature and after heating in air at 300 °C or 500 °C. The symbol * marks the peaks attributed to Cr_2O_5.

Raman spectroscopy is known to be very sensitive to chemical structures and bonding and it was used to complement the XRD data. The results obtained for the various samples are shown in Figure 2. Nickel oxide layers evidenced molecular vibrations corresponding with pure NiO in the first-order transverse optical (1TO) and longitudinal optical (1LO) phonon modes, the second-order 2TO mode and the TO+LO mode [33,34]. The films obtained at a relatively low temperature (as-grown or 300 °C heated) exhibited a hybridized band of 1TO and 1LO phonons, which is typical of a distorted NiO lattice [35]. A decrease of the 1LO phonon energy was related to V_{Ni} defects [36] in agreement with the tensile lattice distortion detected by XRD in the as-grown NiO films. For the chromium oxide layers, Raman shifts were assigned to the A_{1g} and E_g modes of Cr_2O_3 [37]. The signal increment observed at ~650 cm^{-1} for the as-grown sample could be attributed to the forbidden Raman modes of Cr_2O_3 activated in amorphous materials [26,38], which was in accordance with the absence of diffraction peaks in the corresponding XRD pattern (Figure 1). Otherwise, the Raman band that appeared at ~850 cm^{-1} after heating was related to the Cr(VI) states in CrO_3 [39] or Cr_2O_5 [40] forms. For the 300 °C heated sample, the small signal increment around 850 cm^{-1} was related to the Cr_2O_5 phase detected by XRD, which decomposed into Cr_2O_3 and CrO_3 during annealing at 500 °C.

The morphology of the various NiO and Cr_2O_3 layers is illustrated in Figure 3, which includes representative AFM images taken on 2 μm × 2 μm areas together with the respective root-mean-square roughness (r). The images showed smooth and homogeneous films being the surface roughness minimum for the as-grown samples (r < 1 nm) and increased gradually after heating at 300 °C (r ≈ 2 nm) and 500 °C (r ≈ 3 nm). These values were in the same order than those reported for analogous NiO [41–43] and Cr_2O_3 [32,38,44] thin films. The increment of the roughness with the annealing temperature was related to the recrystallization process [32,43] and the consequent enlargement of the mean crystallite

size, as confirmed by the XRD data. Such crystalline enhancement goes together with the agglomeration of grains and the formation of clusters that increase in size as the annealing temperature increases. In addition, undulations appeared on the surface of the layers heated at the highest temperature, as observed in other works [41]. The roughness of the film was related to its crystallinity but could also affect its optical properties because greater roughness could lead to more scattering at the surface and degrade its transparency by increasing the absorption [32]. In any case, all samples had a root-mean-square roughness well below their mean crystallite size indicating that they were flat and compact layers. Therefore, these low values of film roughness are desirable for optoelectronic applications.

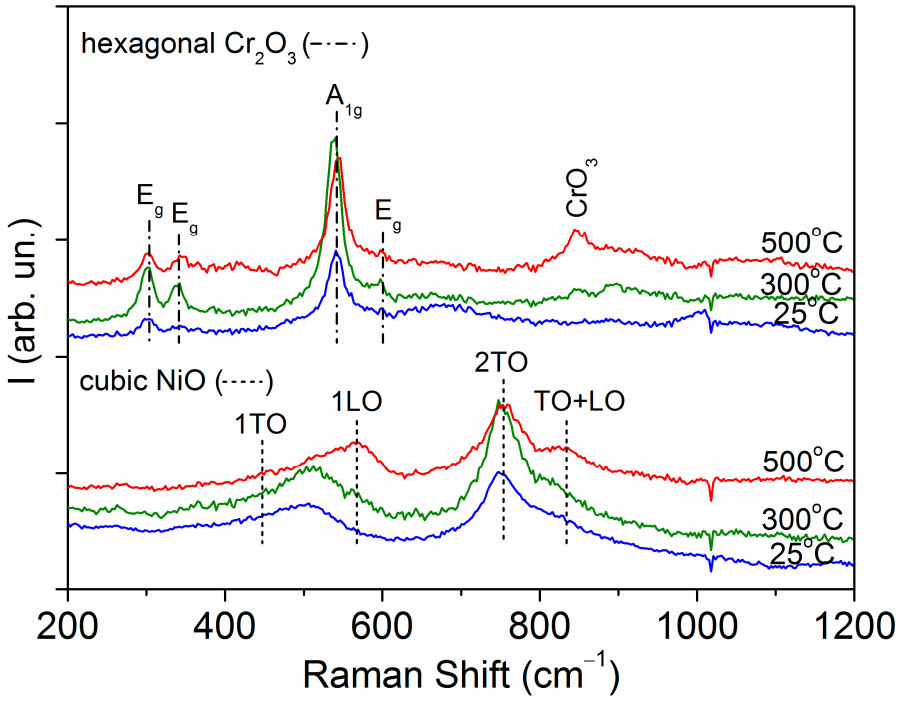

Figure 2. Raman spectra corresponding with the nickel oxide and chromium oxide samples as grown at room temperature and after heating in air at 300 °C or 500 °C.

The optical transmission spectra of the various samples are given in Figure 4. This included the standard photopic vision V(λ), which described the spectral sensitivity of the human eye centered at λ_V = 0.55 μm to better asses the transparency of the films. The visible transmittance (that is, the value T_V taken at λ_V) showed the same evolution for the NiO and Cr_2O_3 layers, increasing from $T_V = 36 \pm 2\%$ for the as-grown films to 54% after heating at 300 °C and higher, to 72%, when the temperature increased to 500 °C. An increment in the visible transmittance with an increasing annealing temperature has been reported for analogous coatings [45–47] with a maximum value around 70% at a 0.55 μm wavelength [46,47]. In general, the optical transmission is expected to depend on various film properties such as impurity centers, surface roughness and level of crystallinity. For these smooth layers, structural defects and interstitial O atoms existing in the as-deposited samples acted as impurities and led to scattering and/or the absorption of incident light. As a result of annealing, the mean crystallite size increased and the interstitial O atoms could diffuse out [45] leading to a decrease in the impurity level and the subsequent increment of the film transmittance with the heating temperature. Furthermore, the coexistence of metal ions in different valence states (Ni^{2+}/Ni^{3+} or Cr^{3+}/Cr^{6+}), which share oxygen anion ligands, allows facile charge transfer processes involving optical absorption in the visible range [23]. The structural data indicated that such coexistence was favored in the as-grown samples but subsequent heating produced an evolution to the most stable valence state.

Both the crystallite size increase and the interstitial O out-diffusion led to the removal of impurity levels and charge transfer processes (that absorbed visible light) after heating, which had a greater effect than roughness on the film transmittance.

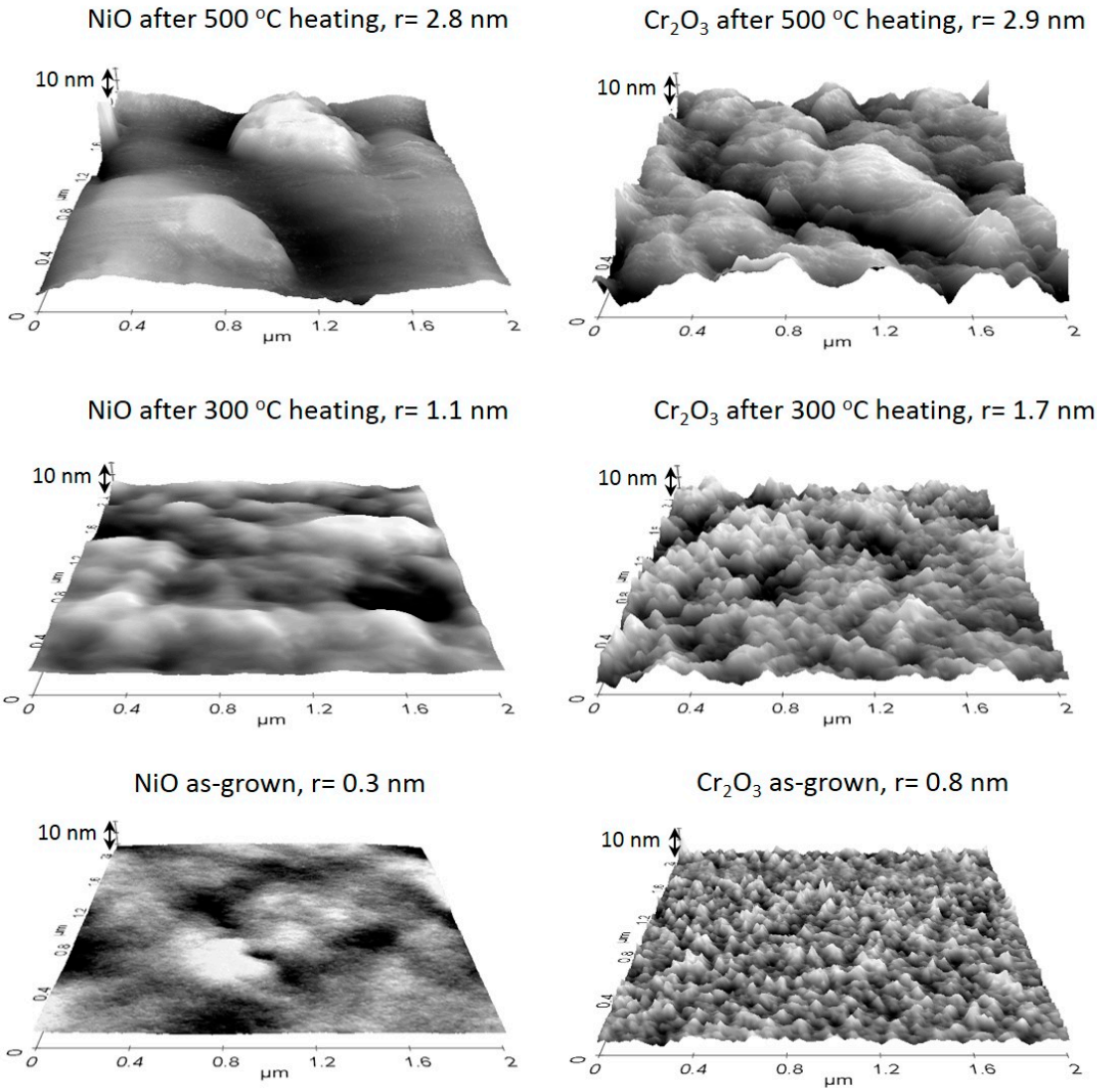

Figure 3. Atomic force microscopy (AFM) images taken on 2 μm × 2 μm areas for the various NiO and Cr_2O_3 layers as-grown and after heating. The root-mean-square roughness (r) is included for each sample.

Figure 5 represents the first derivative of the optical transmittance as a function of the radiation energy for the same spectra shown in Figure 4. The optical gap energy given by the first derivative maximum [22] was clearly identified by prominent peaks in the heated samples, which were in agreement with those expected for the respective material; that is, E_g = 3.70 eV for the NiO films [22,24,46] and E_g = 3.20 eV for the Cr_2O_3 layers [27,47]. The chromium oxide layer heated at 500 °C showed an additional maximum at 2.50 eV, which corresponded with the band gap energy of CrO_3 [48] according to the CrO_3 signal also detected in the Raman spectrum of this sample (in Figure 2). Otherwise, the first derivative maximum appeared less pronounced and shifted towards lower energies in the as-grown layers. The same behavior was observed for other amorphous or poorly crystalline films, which showed a dependence of the band gap energy with the crystallite size and/or with the structural strain. A decrease in the optical gap was noted when the NiO lattice parameter increased and the film turned into tensile strain [14] taking into account that the mean crystallite size decreases with tensile strain as observed here for

the as-deposited NiO. Theoretical calculations indicated that tensile strain would also reduce the gap of Cr_2O_3 [13]. Furthermore, $E_g < 3.2$ eV has been reported for NiO coatings with mean crystallite sizes below 20 nm [49] and $E_g < 2.7$ eV for Cr_2O_3 crystallites below 28 nm [50]. Thus, it can be assumed that the fundamental gap of the crystalline phase and the amorphous phase would be different [31]. Indeed, the near-edge spectrum of amorphous Cr_2O_3 was a slightly broadened version of the single crystal spectrum with a shift of the peaks of ~0.4 eV to lower energies [51]. The origin of the band gap narrowing was then related to structural imperfections (bond angle and distance distortions in relation to defects such as vacancies or interstitials) in the NiO and Cr_2O_3 films obtained at room temperature. For these samples, the decrease in the optical gap energy led to a decrease in visible transmittance.

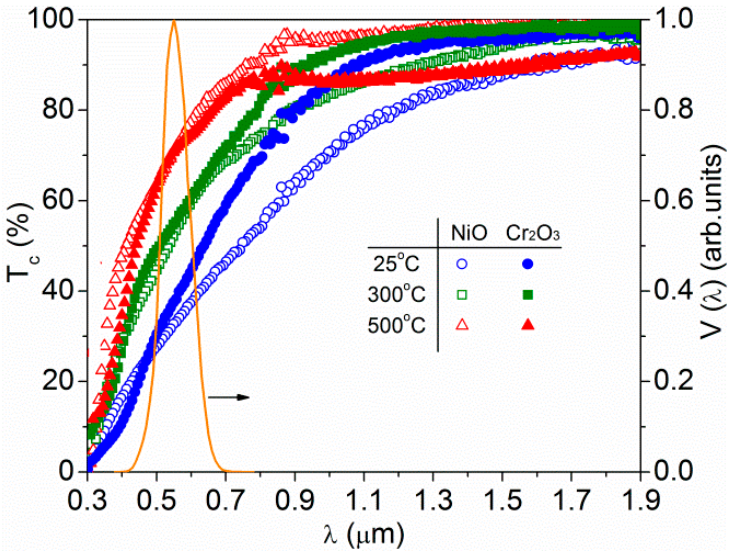

Figure 4. Optical transmittance spectra for the NiO and Cr_2O_3 films as grown at room temperature and after heating in air at 300 °C or 500 °C. The standard photopic vision V(λ), which describes the sensitivity of the human eye, is included for comparison.

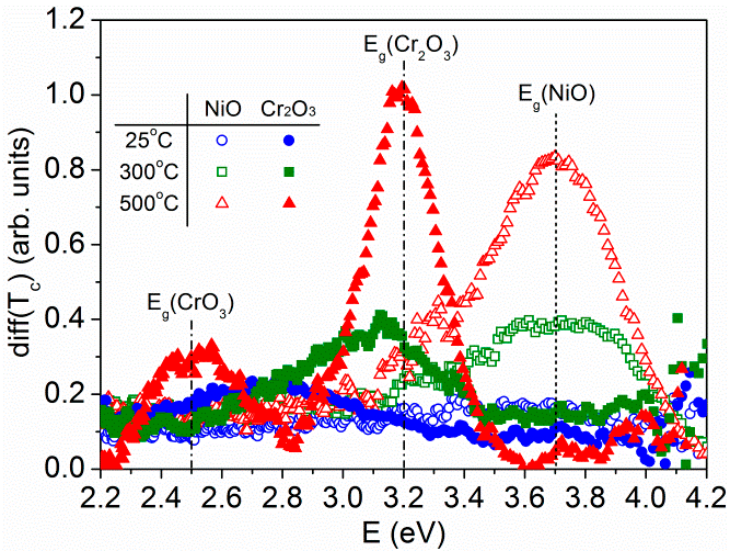

Figure 5. Determination of the optical gap energy for the various NiO and Cr_2O_3 layers from the first derivative of the respective transmittance spectrum in Figure 4.

The electrical data of the sputtered coatings are plotted in Figure 6 as a function of the heating temperature. In all cases, the p-type conductivity was dominated by the concentration of free holes, both being maximum ($\sigma = 2.5 \times 10^{-2}$ S/cm and $N = 2.7 \times 10^{16}$ cm^{-3}) for the unheated NiO film grown at 25 °C. The NiO conductivity decreased to 3.1×10^{-3} S/cm at 300 °C and 8.9×10^{-4} S/cm at 500 °C due to the decrease in the carrier concentration to the 10^{15}–10^{14} cm^{-3} range. The same behavior was observed for other sputtered NiO layers [45,52] when the O-rich plasma induced the incorporation of Ni^{3+} in the lattice and correlatively the formation of nickel vacancies as the previous structural analysis evidenced for the present samples. These nickel vacancies acted as acceptors $(V_{Ni})^{2-}$ that generated holes to fulfill the lattice charge neutrality resulting in the highest conductivity. Nevertheless, the as-grown NiO was thermodynamically unstable and it was easy to release excess oxygen atoms by heat treatment at 300 °C or 500 °C, which produced the out-diffusion of the interstitial oxygen atoms bonded weakly in the sputtered NiO films [52]. Otherwise, the electrical characteristics of Cr_2O_3 remained stable at $\sigma = (4.5 \pm 0.1) \times 10^{-4}$ S/cm and $N = (1.5 \pm 0.2) \times 10^{14}$ cm^{-3} over the entire temperature range. In this case, the incorporation of Cr^{6+} led to the formation of Cr_2O_5 and CrO_3 phases (detected by XRD and Raman spectroscopy) but was less effective in creating chromium vacancy defects that acted as acceptors. The crystallization and disappearance of the disorder-induced Raman mode (at ~ 650 cm^{-1}) did not correlate here with a change in conduction. With regard to the carrier mobility, it is represented in the Figure 6 inset as a function of the respective carrier concentration. It was observed as practically constant at $\mu = 18 \pm 4$ cm^2/Vs for the various layers with $N \leq 10^{15}$ cm^{-3} and decreased to $\mu = 6$ cm^2/Vs for the as-grown NiO with $N = 2.7 \times 10^{16}$ cm^{-3}. These mobility values were within the highest reported for NiO [14,35] and Cr_2O_3 [53] thin films. Depending on the localization length of the holes (L_h) in relation to the lattice constant (a), the conductivity could proceed by hopping (when $L_h < a$) or by a band-like transport (when $L_h > a$) [54]. In the first case, the mobility was expected to be extremely low ($\mu < 0.1$ cm^2/Vs [54]) while the high mobilities observed in the present samples indicated a band-like transport. The lower mobility in the as-grown NiO was due to its higher proportion of defects, which scattered the movement of holes [14]. These sputtered NiO samples exhibited better electrical conduction than Cr_2O_3 for analogous visible transmittance, which is desirable for TCOs. After heating at 500 °C, the NiO films had a sheet resistance $R_s = 1.1 \times 10^5$ kΩ comparable with that achieved by other p-type conductors with a visible transmittance above 70% [6].

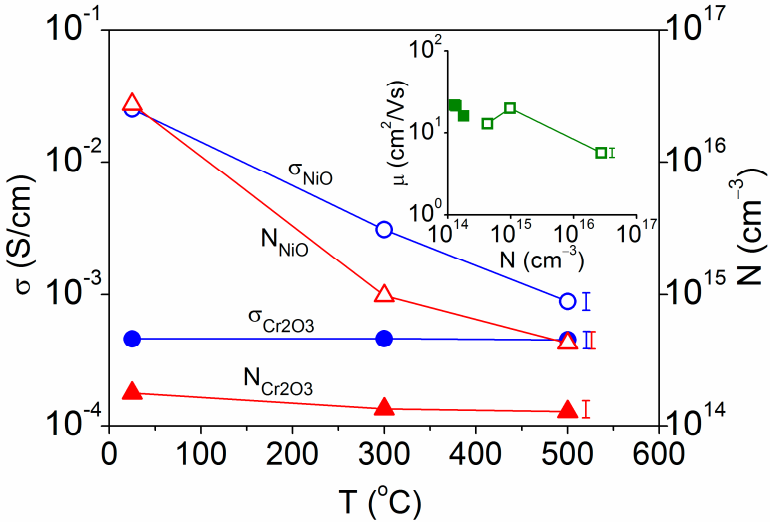

Figure 6. Electrical conductivity and carrier concentration for the NiO and Cr_2O_3 films as a function of the heating temperature. The inset shows carrier mobility versus concentration for the various samples. The error bars are within 5−15% of the mean value. The maximum (15%) is represented on the right, being in the same order as the printed points.

4. Conclusions

NiO and Cr_2O_3 thin films were deposited by reactive DC sputtering on unheated glass substrates and subsequently annealed in air at 300 °C or 500 °C. Beyond their different electronic structure, the optical and electrical characteristics were dominated by the respective structural defects, which could be changed by the heating temperature.

All of the nickel oxide samples showed a cubic NiO structure with some tensile strain in the as-grown conditions and compressive strain after heating. The tensile strain was related to the presence of Ni^{3+} and nickel vacancy defects, which acted as optical absorption centers and charge acceptors $(V_{Ni})^{2-}$. This resulted in a low visible transmittance (34%) and high p-type conductivity (2.5×10^{-2} S/cm) for the as-grown NiO. Nickel vacancy defects, the concentration of holes and conductivity decreased after heating (down to 8.9×10^{-4} S/cm at 500 °C) while the visible transmittance increased (up to 72% at 500 °C).

Otherwise, the chromium oxide layers were amorphous as grown at 25 °C and crystallized into hexagonal Cr_2O_3 at 300 °C or above also with compressive strain after heating. The presence of some Cr^{6+} led to the formation of Cr_2O_5 (at 300 °C) and CrO_3 (at 500 °C) but was less effective in creating chromium vacancy defects that acted as acceptors. Thus, the electrical conductivity remained stable at ~4.5×10^{-4} S/cm over the entire temperature range although the visible transmittance increased with heating in the same way as for NiO.

Author Contributions: Conceptualization, methodology, investigation C.G. and J.H.; formal analysis, writing—original draft preparation C.G.; writing—review and editing C.G. and J.H. All authors have read and agreed to the published version of the manuscript.

Funding: This research received no external funding.

Data Availability Statement: The data are available in this article.

Acknowledgments: This work has been carried out within the internal EFOX (Metal Oxides for Energy Efficiency) project.

Conflicts of Interest: The authors declare no conflict of interest.

References

1. Liu, L.; Cao, K.; Chen, S.; Huang, W. Toward see-through optoelectronics: Transparent light-emitting diodes and solar cells. *Adv. Opt. Mater.* **2020**, *2001122*, 1–31. [CrossRef]
2. Morales-Masis, M.; De Wolf, S.; Woods-Robinson, R.; Ager, J.W.; Ballif, C. Transparent electrodes for efficient optoelectronics. *Adv. Electron. Mater.* **2017**, *3*. [CrossRef]
3. Wang, Z.; Nayak, P.K.; Caraveo-Frescas, J.A.; Alshareef, H.N. Recent developments in p-type oxide semiconductor materials and devices. *Adv. Mater.* **2016**, *28*, 3831–3892. [CrossRef] [PubMed]
4. Woods-Robinson, R.; Broberg, D.; Faghaninia, A.; Jain, A.; Dwaraknath, S.S.; Persson, K.A. Assessing high-throughput descriptors for prediction of transparent conductors. *Chem. Mater.* **2018**, *30*, 8375–8389. [CrossRef]
5. Buckeridge, J.; Catlow, C.R.A.; Farrow, M.R.; Logsdail, A.J.; Scanlon, D.O.; Keal, T.W.; Sherwood, P.; Woodley, S.M.; Sokol, A.A.; Walsh, A. Deep vs shallow nature of oxygen vacancies and consequent n -type carrier concentrations in transparent conducting oxides. *Phys. Rev. Mater.* **2018**, *2*, 56–59. [CrossRef]
6. Hu, L.; Wei, R.H.; Tang, X.W.; Lu, W.J.; Zhu, X.B.; Sun, Y.P. Design strategy for p-type transparent conducting oxides. *J. Appl. Phys.* **2020**, *128*, 140902. [CrossRef]
7. Hu, L.; Zhao, M.L.; Liang, S.; Song, D.P.; Wei, R.H.; Tang, X.W.; Song, W.H.; Dai, J.M.; He, G.; Zhang, C.J.; et al. Exploring high-performance p-type transparent conducting oxides based on electron correlation in V_2O_3 thin films. *Phys. Rev. Appl.* **2019**, *12*, 1–9. [CrossRef]
8. Yamaguchi, K.; Nakano, M.; Namimoto, H.; Fueno, T. Extended Hubbard models for transition metal oxides and halides: Importance of spin and charge fluctuations in charge transfer metals. *Jpn. J. Appl. Phys.* **1988**, *27*, L1835–L1838. [CrossRef]
9. Shih, B.C.; Abtew, T.A.; Yuan, X.; Zhang, W.; Zhang, P. Screened Coulomb interactions of localized electrons in transition metals and transition-metal oxides. *Phys. Rev. B-Condens. Matter Mater. Phys.* **2012**, *86*, 1–8. [CrossRef]
10. Fujimori, A.; Yoshida, T.; Okazaki, K.; Tsujioka, T.; Kobayashi, K.; Mizokawa, T.; Onoda, M.; Katsufuji, T.; Taguchi, Y.; Tokura, Y. Electronic structure of Mott-Hubbard-type transition-metal oxides. *J. Electron Spectros. Relat. Phenomena* **2001**, *117–118*, 277–286. [CrossRef]
11. Zimmermann, R.; Steiner, P.; Claessen, R.; Reinert, F.; Hüfner, S.; Blaha, P.; Dufek, P. Electronic structure of 3d-transition-metal oxides: On-site Coulomb repulsion versus covalency. *J. Phys. Condens. Matter* **1999**, *11*, 1657–1682. [CrossRef]

12. Guillén, C.; Herrero, J. Transparent and p-type conductive Ni_xO:V thin films obtained by reactive DC sputtering at room temperature. *Mater. Res. Express* **2019**, *6*, 96410. [CrossRef]
13. Mi, Z.; Chen, L.; Shi, C.; Ma, Y.; Wang, D.; Li, X.; Liu, H.; Qiao, L. The effects of strain and vacancy defects on the electronic structure of Cr_2O_3. *Comput. Mater. Sci.* **2018**, *144*, 64–69. [CrossRef]
14. Hwang, J.D.; Ho, T.H. Effects of oxygen content on the structural, optical, and electrical properties of NiO films fabricated by radio-frequency magnetron sputtering. *Mater. Sci. Semicond. Process.* **2017**, *71*, 396–400. [CrossRef]
15. Park, S.; Ahn, H.S.; Lee, C.K.; Kim, H.; Jin, H.; Lee, H.S.; Seo, S.; Yu, J.; Han, S. Interaction and ordering of vacancy defects in NiO. *Phys. Rev. B Condens. Matter Mater. Phys.* **2008**, *77*. [CrossRef]
16. Medasani, B.; Sushko, M.L.; Rosso, K.M.; Schreiber, D.K.; Bruemmer, S.M. Vacancies and vacancy-mediated self diffusion in Cr_2O_3: A first-principles study. *J. Phys. Chem. C* **2017**, *121*, 1817–1831. [CrossRef]
17. Tang, C.-J.; Ye, J.-M.; Yang, Y.-T.; He, J.-L. Large-area flexible monolithic ITO/WO_3/Nb_2O_5/NiVOχ/ITO electrochromic devices prepared by using magnetron sputter deposition. *Opt. Mater.* **2016**, *55*, 83–89. [CrossRef]
18. Egorova, K.S.; Ananikov, V.P. Toxicity of metal compounds: Knowledge and myths. *Organometallics* **2017**, *36*, 4071–4090. [CrossRef]
19. Contoux, G.; Cosset, F.; Célérier, A.; Machet, J. Deposition process study of chromium oxide thin films obtained by d.c. magnetron sputtering. *Thin Solid Films* **1997**, *292*, 75–84. [CrossRef]
20. Lin, J.; Sproul, W.D. Structure and properties of Cr_2O_3 coatings deposited using DCMS, PDCMS, and DOMS. *Surf. Coat. Technol.* **2015**, *276*, 70–76. [CrossRef]
21. Hong, W.Q. Extraction of extinction coefficient of weak absorbing thin films from special absorption. *J. Phys. D. Appl. Phys.* **1989**, *22*, 1384–1385. [CrossRef]
22. Garoufalis, C.S.; Barnasas, A.; Stamatelatos, A.; Karoutsos, V.; Grammatikopoulos, S.; Poulopoulos, P.; Baskoutas, S. A study of quantum confinement effects in ultrathin NiO films performed by experiment and theory. *Materials* **2018**, *11*, 949. [CrossRef]
23. Miedzinska, K.M.E.; Hollebone, B.R.; Cook, J.G. Optical properties and assignment of the absorption spectra of sputtered mixed valence nickel oxide films. *J. Phys. Chem. Solids* **1988**, *49*, 1355–1362. [CrossRef]
24. Mendoza-Galván, A.; Vidales-Hurtado, M.A.; López-Beltrán, A.M. Comparison of the optical and structural properties of nickel oxide-based thin films obtained by chemical bath and sputtering. *Thin Solid Films* **2009**, *517*, 3115–3120. [CrossRef]
25. Zhu, M.; Li, F.; Zhou, G.; Jin, X.; Wang, X.; Wang, L.; Song, F. Microstructures and electrical properties of nanostructured Cr_2O_3 thin films deposited by dual-target reactive high-power impulse magnetron sputtering. *Vacuum* **2019**, *164*, 293–299. [CrossRef]
26. Mohammadtaheri, M.; Yang, Q.; Li, Y.; Corona-Gomez, J. The effect of deposition parameters on the structure and mechanical properties of chromium oxide coatings deposited by reactive magnetron sputtering. *Coatings* **2018**, *8*, 111. [CrossRef]
27. Abdullah, M.M.; Rajab, F.M.; Al-Abbas, S.M. Structural and optical characterization of Cr_2O_3 nanostructures: Evaluation of its dielectric properties. *AIP Adv.* **2014**, *4*. [CrossRef]
28. Hewston, T.A.; Chamberland, B.L. Magnetic and structural studies of Cr_2O_5 and Cr_3O_8. *J. Magn. Magn. Mater.* **1984**, *43*, 89–95. [CrossRef]
29. Ivanov, P.G.; Watts, S.M.; Lind, D.M. Epitaxial growth of CrO_2 thin films by chemical-vapor deposition from a Cr_8O_{21} precursor. *J. Appl. Phys.* **2001**, *89*, 1035–1040. [CrossRef]
30. Si, P.Z.; Wang, H.X.; Jiang, W.; Lee, J.G.; Choi, C.J.; Liu, J.J. Synthesis, structure and exchange bias in Cr_2O_3/CrO_2/Cr_2O_5 particles. *Thin Solid Films* **2011**, *519*, 8423–8425. [CrossRef]
31. Gago, R.; Vinnichenko, M.; Hübner, R.; Redondo-Cubero, A. Bonding structure and morphology of chromium oxide films grown by pulsed-DC reactive magnetron sputter deposition. *J. Alloys Compd.* **2016**, *672*, 529–535. [CrossRef]
32. Hones, P.; Diserens, M.; Lévy, F. Characterization of sputter-deposited chromium oxide thin films. *Surf. Coat. Technol.* **1999**, *120–121*, 277–283. [CrossRef]
33. Dietz, R.E.; Parisot, G.I.; Meixner, A.E. Infrared absorption and Raman scattering by two-magnon processes in NiO. *Phys. Rev. B* **1971**, *4*, 2302–2310. [CrossRef]
34. De Los Santos Valladares, L.; Ionescu, A.; Holmes, S.; Barnes, C.H.W.; Bustamante Domínguez, A.; Avalos Quispe, O.; González, J.C.; Milana, S.; Barbone, M.; Ferrari, A.C.; et al. Characterization of Ni thin films following thermal oxidation in air. *J. Vac. Sci. Technol. B Nanotechnol. Microelectron. Mater. Process. Meas. Phenom.* **2014**, *32*, 51808. [CrossRef]
35. Ono, M.; Sasaki, K.; Nagai, H.; Yamaguchi, T.; Higashiwaki, M.; Kuramata, A.; Yamakoshi, S.; Sato, M.; Honda, T.; Onuma, T. Relation between electrical and optical properties of p-type NiO films. *Phys. Status Solidi Basic Res.* **2018**, *255*, 1–5. [CrossRef]
36. Wang, M.; Thimont, Y.; Presmanes, L.; Diao, X.; Barnabé, A. The effect of the oxygen ratio control of DC reactive magnetron sputtering on as-deposited non stoichiometric NiO thin films. *Appl. Surf. Sci.* **2017**, *419*, 795–801. [CrossRef]
37. Shim, S.H.; Duffy, T.S.; Jeanloz, R.; Yoo, C.S.; Iota, V. Raman spectroscopy and x-ray diffraction of phase transitions in Cr_2O_3 to 61 GPa. *Phys. Rev. B-Condens. Matter Mater. Phys.* **2004**, *69*, 1–12. [CrossRef]
38. Barshilia, H.C.; Rajam, K.S. Growth and characterization of chromium oxide coatings prepared by pulsed-direct current reactive unbalanced magnetron sputtering. *Appl. Surf. Sci.* **2008**, *255*, 2925–2931. [CrossRef]
39. Kikuchi, S.; Kawauchi, K.; Kurosawa, M.; Honjho, H.; Yagishita, T. Non-destructive rapid analysis discriminating between chromium(VI) and chromium(III) oxides in electrical and electronic equipment using Raman spectroscopy. *Anal. Sci.* **2005**, *21*, 197–198. [CrossRef]

40. Monnereau, O.; Tortet, L.; Grigorescu, C.E.A.; Savastru, D.; Iordanescu, C.R.; Guinneton, F.; Notonier, R.; Tonetto, A.; Zhang, T.; Mihailescu, I.N.; et al. Chromium oxides mixtures in PLD films investigated by Raman spectroscopy. *J. Optoelectron. Adv. Mater.* **2010**, *12*, 1752–1757.
41. Zhuang, S.; He, J.; Ma, X.; Zhao, Y.; Wang, H.; Zhang, B. Fabrication and optimization of hole transport layer NiO for all inorganic perovskite light emitting diodes. *Mater. Sci. Semicond. Process.* **2020**, *109*, 104924. [CrossRef]
42. Keraudy, J.; García Molleja, J.; Ferrec, A.; Corraze, B.; Richard-Plouet, M.; Goullet, A.; Jouan, P.Y. Structural, morphological and electrical properties of nickel oxide thin films deposited by reactive sputtering. *Appl. Surf. Sci.* **2015**, *357*, 838–844. [CrossRef]
43. Hotovy, I.; Huran, J.; Spiess, L. Characterization of sputtered NiO films using XRD and AFM. *J. Mater. Sci.* **2004**, *39*, 2609–2612. [CrossRef]
44. Özen, S.; Şenay, V. Optical, morphological and nano-mechanical properties of chromium oxide thin films fabricated by radio frequency (RF) magnetron sputtering. *Optik* **2020**, *201*. [CrossRef]
45. Yang, J.L.; Lai, Y.S.; Chen, J.S. Effect of heat treatment on the properties of non-stoichiometric p-type nickel oxide films deposited by reactive sputtering. *Thin Solid Films* **2005**, *488*, 242–246. [CrossRef]
46. Atak, G.; Coşkun, Ö.D. Annealing effects of NiO thin films for all-solid-state electrochromic devices. *Solid State Ionics* **2017**, *305*, 43–51. [CrossRef]
47. Singh, J.; Verma, V.; Kumar, R.; Kumar, R. Structural, optical and electrical characterization of epitaxial Cr_2O_3 thin film deposited by PLD. *Mater. Res. Express* **2019**, *6*, 106406. [CrossRef]
48. Zhai, H.-J.; Li, S.; Dixon, D.A.; Wang, L.-S. Probing the electronic and structural properties of chromium oxide clusters $(CrO_3)_n^-$ and $(CrO_3)_n$ (n = 1–5): Photoelectron spectroscopy and density functional calculations. *J. Am. Chem. Soc.* **2008**, *130*, 5167–5177. [CrossRef] [PubMed]
49. Makhlouf, S.A.; Kassem, M.A.; Abdel-Rahim, M.A. Crystallite size-dependent optical properties of nanostructured NiO films. *Optoelectron. Adv. Mater. Rapid Commun.* **2010**, *4*, 1562–1568.
50. Ekwealor, A.B.C. Variations of optical and structural properties with temperature for Cr_xO_y thin films synthesized in a polymer matrix by chemical bath deposition technique. *Dig. J. Nanomater. Biostruct.* **2014**, *9*, 423–431.
51. Kucheyev, S.O.; Sadigh, B.; Baumann, T.F.; Wang, Y.M.; Felter, T.E.; van Buuren, T.; Gash, A.E.; Satcher, J.H.; Hamza, A.V. Electronic structure of chromia aerogels from soft X-ray absorption spectroscopy. *J. Appl. Phys.* **2007**, *101*, 124315. [CrossRef]
52. Karsthof, R.; Anton, A.M.; Kremer, F.; Grundmann, M. Nickel vacancy acceptor in nickel oxide: Doping beyond thermodynamic equilibrium. *Phys. Rev. Mater.* **2020**, *4*, 1–9. [CrossRef]
53. Singh, J.; Kumar, R.; Verma, V.; Kumar, R. Structural and optoelectronic properties of epitaxial Ni-substituted Cr2O3 thin films for p-type TCO applications. *Mater. Sci. Semicond. Process.* **2020**, 105483. [CrossRef]
54. Bosman, A.J.; van Daal, H.J. Small-polaron versus band conduction in some transition-metal oxides. *Adv. Phys.* **1970**, *19*, 1–117. [CrossRef]